# Microwave Imaging of Biological Tissues: the current status in the research area

Tommy Gunnarsson *

December 18, 2006

*Department of Computer Science and Electronics, Mälardalen University

**Abstract**

Microwave imaging is a non-ionizing method promising an ability of depth-scanning different biological bodies. The research in this area started in the late 70s and many contributions has been achieved by different groups until present, which have influenced and open up new possibilities of the technique. This document will review the historical work by the different groups to settle objectives of the research in microwave imaging at the Department of Computer Science and Electronics at Mälardalen University and the plan of the author's Ph. D. studies. The planar 2.45 GHz microwave camera located at Supélec, France, may be a very useful platform in early studies of the three-dimensional properties of microwave imaging for breast tumor detection. By applying the developed Newton-Kantorovich algorithm to the planar camera a solid state of the art platform for quantitative reconstruction of inhomogeneous objects may be established.

# Contents

# 1 Introduction

Microwave imaging is a non-ionizing method which promises the ability of depth-scanning different dielectric bodies for biomedical applications. This method has been proved able to detect malignant tumors as the dielectric properties of these differ from other human tissues. The contrast in permittivity for different in-vivo tissues (bone, fat, malign tumor, vascular tissue etc.) is much higher compared to the density contrast X-Ray Computed Tomography (CT) can yield [1]. For this reason, microwave imaging has been developed as a complementary modality to mammography[2, 3]. However, microwave imaging needs a improvements in both hardware platforms and imaging algorithms to be considered as a reliable and quantitative modality for biomedical application. The complexity of biomedical tissues makes the wave propagation complicated and demanding high sensitivity in the hardware. The scattering phenomenon in microwave imaging is highly non-linear and demands a great amount of calculation capabilities to reconstruct an image with reasonable quality. Impressive results in inverse scattering algorithms for two-dimensional scenarios have been obtained by [1, 4, 5, 6], resulting in tomographic imaging of bodies with complex dielectric permittivity[1, 5, 7, 68, 69]. The tomographic algorithms must be further developed to improve the convergence of the inverse problem and a more stable platform must be established before the technique can be considered as a useful complementary technique in the biomedical area.

In this document earlier research in the area of microwave imaging of biological tissues will be reviewed and summarized, from the beginning of the 80s until present. First the hardware development will be discussed, followed by the algorithm development. In the end, the specific phantom model developing for the breast tumor detection application is discussed. The last section points out some possible future directions in this area.

# 2 Developed Hardware Setups

Several hardware setups have been developed during the last three decades. The first successful experiments where performed by Larsen and Jacobi in the late 70s, resulting in images showing the internal structures of canine kidneys. These experiments where made, using two antennas and measuring the transmission coefficients between them with a mechanical rotation around the object [10]. These results constructed a major foundation opening up the future of microwave imaging of biological tissues.

## 2.1 Microwave Tomography Systems Performing in Frequency-Domain

### 2.1.1 The Planar Microwave Camera

One of the first imaging systems developed was the planar microwave camera by Bolomey *et al.* during the 80s. This planar microwave camera includes two large horn-antennas, one transmitter and one receiver, with a water tank in between. The transmitting antenna is designed to produce an approximately plane wave which is received in the receiving antenna, depicted in Figure 1. The object is immersed of water into the water tank and the scattered field due to the object is measured along a plane behind the object. The camera using 1024 dipole antennas on a plane matrix placed on the water tank in front of the receiving horn antenna, also named the collector. The antenna matrix forms a syntectic retina where the antenna elements distributing the plane-wave passing it. The retina is not considered as a receiver while it disturbs the field before the receiving collector in a Modulated Scattering Technique(MST) fashion[11]. Using this technique one antenna element is active at the time by a modulation of 200 kHz, the received signal in the collector gives information of the field properties at the antenna element position. By scanning through all elements of the retina quick data acquisition is archived using a relatively simple hardware[12]. This because the retina elements is modulated by a frequency of 200 kHz, which modulates the planar carrier wave frequency of 2.45 GHz, only two high frequency channels is needed for 1024 measurements points.

Using lower frequency the multiplexer controlling the sensor matrix may be simplified. This camera was developed with the main goal to produce qualitative images of the temperature distribution of biological tissues to control the effect during hyperthermia treatment [13, 14]. The camera has been further developed since then to produce quantitative results [15] as well as qualitative results in a quasi real-time manner [16]. Ann Franchois was able to produce quantitative results of a homogenous cylinder, with the conclusion that the calibration of the incident field was one of the main issues to improve the quantitative result [15]. While a quasi real-time acquisition time of the image is a useful issue in many biological applications Alain Joisel have further developed the real-time functionality of the

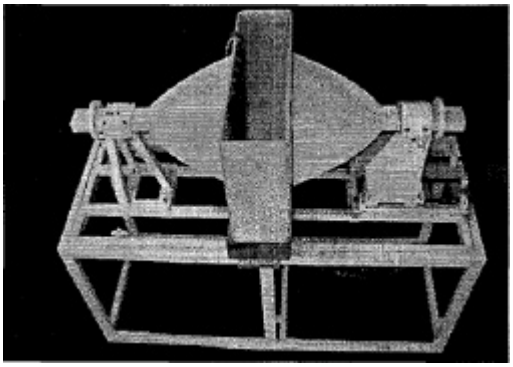

Figure 1: Microwave planar camera developed by Bolomey *et al.* [12].

system. In [16] qualitative results have been reported with a rate of 15 images/sec.

### 2.1.2 The 64 Antenna Circular Microwave Camera

In parallel with the later part of the planar camera development Jofre *et al.* developed the first circular microwave camera able to do multi-view measurements without mechanical movements. The microwave camera operates at a frequency of 2.45 GHz using 64 horn-antennas operating in $TE_{10}$ mode, arranged in a circle with a diameter of 25 cm, depicted in Figure 2. The antennas is used in both transmitting and receiving mode, with one transmitting antenna at the time and measuring the scattered field at the opposite 33 antennas. By changing transmitting antenna around the circle a rotation around the object may be done electrically. This is one of the major advantages of this circular setup compared to the Bolomey *et al.* planar setup and Jacobi *et al.* mechanical system. A transmitting/receiving multiplexer for 2.45 GHz signals is a challenging issue to develop. In this case the antennas are divided into four one-to-16 multiplexors, created by trees of PIN diodes [17]. These four multiplexors is then connected to the transmit/receive equipment through a two- to four-way switching matrix. However, the leakage between the transmitting and receiving part requires a non-practical isolation. The isolation problem is solved by using a low-frequency modulation to separate the useful signals from interferences[18]. A double amplitude modulation is archived close the transitter/receiver antennas together with a demodulation in the data acquisition unit, through this process the wanted signal path is isolated trough . This equipment is able to measure 64 views around an object in 3 s, but using averaging to reduce noise in the measurements one measurement cycle takes about 45 s.

This equipment was also used to produce qualitative results in the beginning using the diffraction tomography algorithm [18], but have also been used to obtain data for iterative algorithms for quantitative results at a lower operating frequency

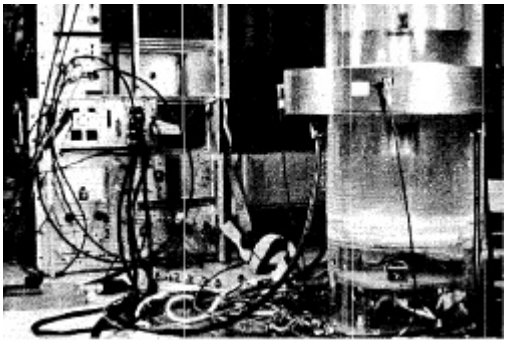

Figure 2: The circular microwave camera developed by Jofre *et al.* with 64 transmitting/receiving horn-antennas [12, 17, 18].

of 2.33 GHz [5, 7, 69, 71]. Using an iterative non-linear algorithm the resolution is not limited to $\lambda/2$ as in the diffraction tomography case, using a priori information the resolution may be improved. However, the result is highly dependent of the SNR of the system [7]. In [7] a SNR of 20 dB was obtained in the system and still quantitative results of a human forearm was archived with good convergence.

### 2.1.3 The 32/32 Antenna Circular Microwave Scanner

In the mid 90s Semenov *et al.* developed a 64 antenna circular microwave scanner using waveguide-antennas operating on a frequency of 2.45 GHz [20]. This system is based upon a cylindrical cavity with a diameter of 37 cm, depicted in Figure 3. at this time it was well known that creating a system with antennas able to alternate between transmitting and receiving mode causes a major isolation problem between the channels. Therefore this group divided the antennas between 32 transmitting antennas and 32 receiving antennas with separate transmitt/receive channels. However this is of course a step backwards in number of possible input data for the algorithms, compared to the barcelona setup.

The waveguide-antennas are constructed with a three time wider field pattern in the horizontal plane compared to the vertical plane. The dimensions of the antenna is 30 mm*9 mm operating in $TE_{10}$ mode. With this system they tried to use a 2-D model of the diffraction to create 2-D images slicing a 3-D object. However, they conclude in [20] that it is not successful to slice a 3-D object using a 2-D model. They propose that a 3-D object should be reconstructed in as a fully 3-D structure in a 3-D model to avoid 3-D artifacts, but the final result may then be visualized as a 2-D sliced image of structure [20]. Note, that a 3-D structure containing spatial and dielectric variations along the vertical axis, if a 2-D model is used for the image reconstruction those variations are not including causing artifacts in the reconstructed image. Using this system Semenov *et al.* produced qualitative result

in quasi real-time of a beating canine heart with a data acquisition from all 32 transmitting antennas around the object in less than 500 ms. They summarize that a 3-D model is needed to create quantitative results of a biomedical object as in their study of a heart [20].

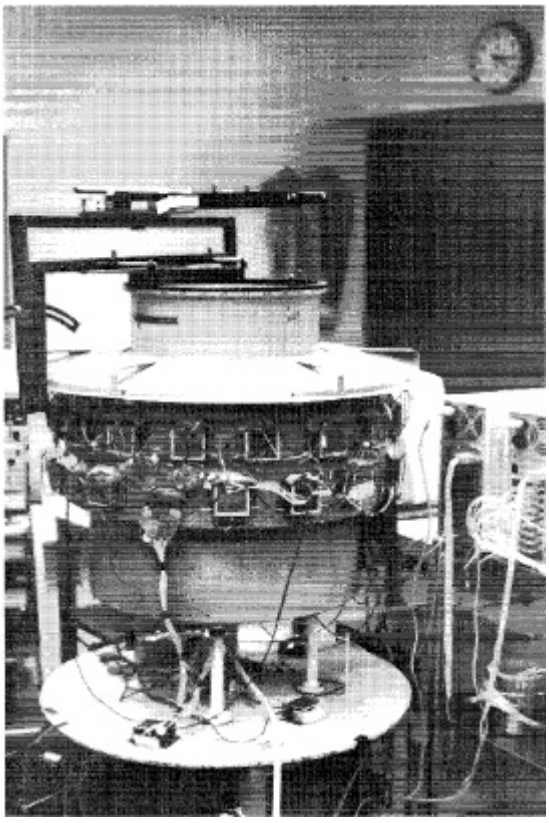

Figure 3: The circular microwave camera developed by Semenov *et al.* with 32 transmitting and 32 receiving waveguide-antennas [20].

### 2.1.4 The Clinical Circular Prototype Scanner for Biological Imaging

In parallel with the Semenov *et al.* Meaney *et al.* started their development of a circular microwave imaging system for reconstruction of 2-D electrical property distributions. In their first system 8 antennas were used. Four transmitting waveguide antennas and 4 receiving monopole antennas. The system operates on a frequency-band between 300 - 1100 MHz. The motivation for a multi-frequency system was that the system could be used in a experimental investigation to find the optimal

frequency for the imaging process as well using different frequencies to improve image quality and the system's usability[21]. The antenna system operates in the TM mode, where the most of the E-field is assumed to be vertical polarized. This data acquisition system also use amplitude modulation to increase the isolation between the transmitting and receiving channel.

The long term objective of this system is also the thermal imaging during hyperthermia treatment, like Bolomey and Jofre *et al.*. At this time no group had been able to produce experimental quantitative results of the temperature inside larger objects with high dielectric contrast, using the quasi real-time diffraction tomography methods. Only the differential issue of temperature differences without quantitative information had been obtained [17]. The approach for Meany *et al.* was to develop a system able produce static quantitative images of biological tissues. For this reason they started with an iterative inverse scattering method which is more time-consuming than the earlier spectral diffraction methods [6]. The algorithm used was developed from the Newton-based method using a hybrid of the Finite Element and the Boundary Element method to compute the electric field at each iteration [22, 23]. This to lower the number of unknowns and lowering the calculation effort in the forward solver. In this step the quasi real-time functionality is lost but what is gained is the ability to handle more complex objects with many scatterers and high electrical property variations. In [21] the first experimental results are presented together with a calibration technique. In this early step quantitative results where produced for objects with an approximate size of one-half wavelength.

This setup was further developed in the late 90s with a circular antenna array with a diameter of 25 cm containing 32 monopole-antennas. In this setup the monopole-antennas where used as both transmitters and receivers in the TM-mode using the same data acquisition system as in the earlier system, depicted in Figure 4. One antenna is a transmitter while the other antennas can act as receivers, so a circular scan is performed by changing transmitting antenna along the the circle in the same manner as the Jofre *et al.* system [24]. The paper describes how the imaging result is improved while a simpler transmitting antenna is used. This is mainly because the monopole antenna is easier to model. The forward solution gives a better result in the comparison with the experimental measurement, which in fact improves the convergence of the imaging algorithm. They propose to use monopole-antennas with the motivation that it is possible to locate the object in the near-field region and still get an acceptable field pattern inside the object. A waveguide-antenna have better antenna gain but need some non-interfering space in the near-field region. Using only monopole-antennas the system may be minimized around the object and some of the losses in SNR due to the lack of antenna gain is regained, due to the shorter distance between the transmitting and the receiving antenna. Improved results are achieved in both the real and imaginary part of the permittivity in a comparison to the earlier waveguide system [24]. Furthermore, the monopole-antenna may be easily modeled as a line source. A new kind of

calibration is also proposed which is useful for all antenna types. This calibration technique improved the result even more[24].

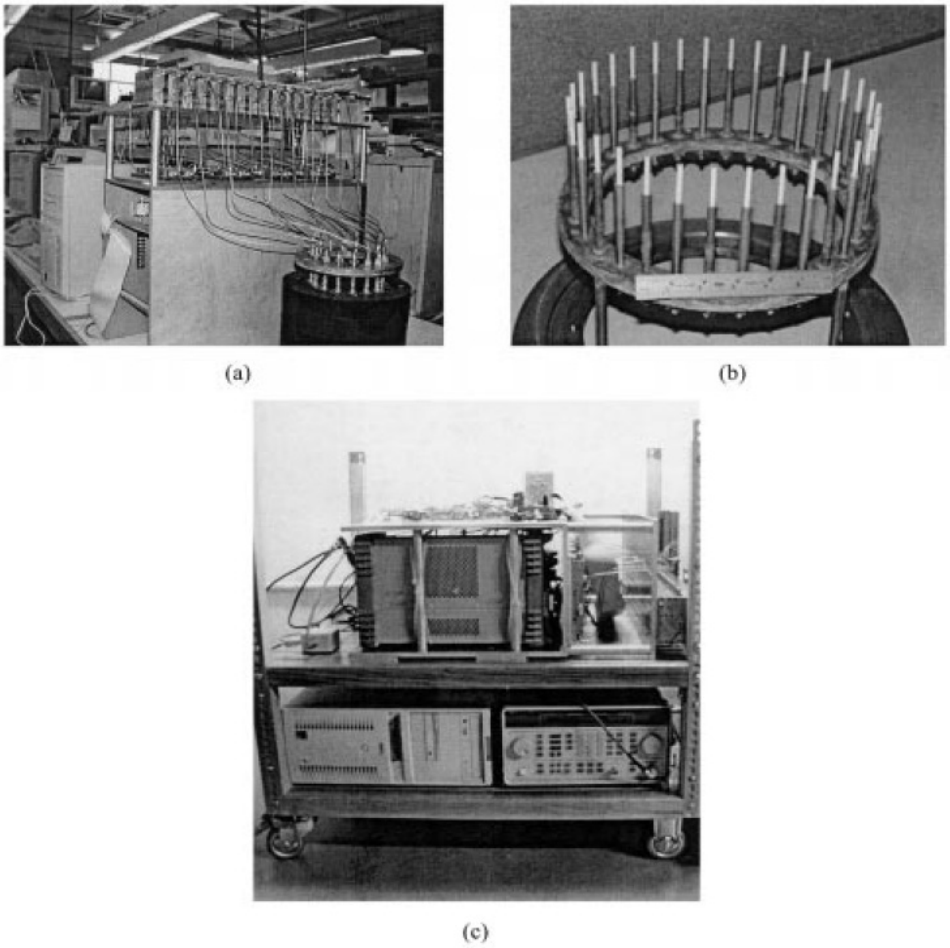


Figure 4: The active microwave circular camera for imaging of biological materials, developed by Meaney *et al.* [21, 24]. (a) The tank with the 32-channel data acquisition system in laboratory operation. (b) View of the 32 monopole-antenna array. (c) A view of the data acquisition system mounted on a transportable chart.

The first clinical prototype for active microwave imaging of the breast was developed in the early 2000s by Meaney *et al.* [25]. The objective of this system is quantitative images of the breast to detect early stage breast tumors. The system is based on the earlier developed system where the system is mounted on a

transportable bed with a hole for the breast insertion, see Figure 5. In this case they only use 16 of the 32 available channels in the system by using a smaller 16 antenna circular array with the diameter of 15 cm. In the study [25] breast images of 5 real patients with different ages is performed. One session lasted between 10-15 min per breast, where the data acquisition at seven different antenna heights with seven different frequencies at each antenna array height was included. The initial results gives sliced 2-D images of the human breast with a reasonable resolution. It is clearly shown that the permittivity of the breast tissues differs between different patients and with the age of the patient. This was explained to correlate with the amount of fatty tissues compared to the glandular and fibrous tissues. They also propose that the *in vivo* tissues have a higher permittivity compared to the published *ex vivo* studies. In this setup the nonactive antennas where modeled as microwave sinks so the entering E-field is absorbed and not re-radiated [62][63]. In the hardware they are using matched switches so when an antenna is in nonactive stage any entering signal is transferred trough the coax-cables into the switch with a matched termination, which eliminates the re-radiation.

Figure 5: The clinical prototype for active microwave imaging of the breast in application of breast tumor detection, developed by Meaney *et al.* [25].

Many improvements on the system's software has then be done, while using the same hardware. One approach is to use the unwrapped phase in the imaging algorithm instead of using only the limited $2\pi$ phase shift in one Rieman sheet in the complex plane [28]. This improves the image quality while imaging high-contrast

objects without the same demands of the a priori information about object size and permittivity. Further, the measured log magnitude is used directly in their algorithms, which improves the error-rate in the measured data [3]. Using this system studies has been done of the 3-D artifacts caused while using a 2-D model of a 3-D object [29], while the iterative algorithm is a fully 2-D algorithm. With the experience from these studies a scalar 3-D/2-D algorithm has been implemented [1] to lower the 3-D artifacts in the 2-D imaging. Furthermore, improved image quality has also been accomplished by finding the boundary of the object. If the exact boundary is found it is then possible to model the boundary properties as a step function, while the surrounding medium is known [2]. In this method, first, the object boundary must be fond to adjust the size of the FE-region to fit the object with heterogenous medium. Outside this region the homogeneous medium is modeled using the boundary element method. In [2] it is shown that this method improves the images, especially if the inhomogeneities is located near the boundary of the object. Finally, Meaney *et al.* have done some effort to produce a new prototype system with a frequency band of 0.5 – 3 GHz [30]. Using this system the group has been able to produce images of a breast using a frequency band between 600 MHz – 2.1 GHz. The bandwidth is limited by the dynamic degradation of the data acquisition system and by the high attenuation of the lossy medium at higher frequencies. One important point of their contribution is the fact that a simple antenna, as a monopole antenna, can be used with success in this context with a fairly wide band and simple models.

### 2.1.5 The 434 MHz Circular Microwave Scanner

In the late 90s Geffrin *et al.* developed a circular scanner operating at a frequency of 434 MHz. This configuration consists of 64 antennas attached inside a metallic cylinder with a diameter of 59 cm [31, 32]. This setup was intended to be able to perform a full-body scan of the human body, but may be useful in other applications as well. Under the development the camera where equipped with 64 printed circuit H-type E-polarized antennas [31]. However, the final version is equipped with 64 biconical antennas [32], depicted in Figure 6. This is the first developed microwave scanner with a metal enclosure, which of course having both advantages and disadvantages. This system is surrounded by a metallic cylinder. The metallic enclosure will increase the standing wave pattern outside the object and the coupling affect between the enclosure and the antennas. Earlier non-metallic enclosures made a infinity approximation useable in the algorithms while using lossy immersion medium, where all secondary effects are suppressed. While this metallic surrounded scenario must use a metallic boundary in a finite description of the equipment including the reflection effects and the standing wave pattern in the region between the metallic wall and the object. This choice increasing the computation effort, however, this system is more stable with a more shielded and well defined environment. Approximating the environment as an cavity of infinite height, many simplifications may be

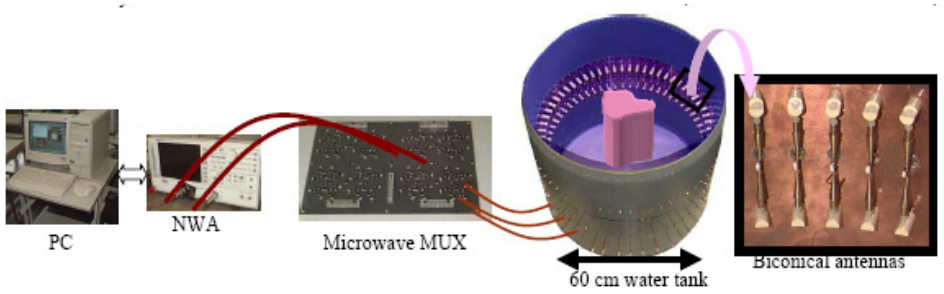


Figure 6: The circular 434 MHz microwave scanner developed by Geffrin *et al.* [32].

done when the standing wave pattern outside the object is not an issue and in many cases the effect from the unused antennas may be neglected with a satisfactory result. Ann Franchois has developed a Newton-type 2-D reconstruction algorithm for this system, where the antenna integration and the effects of the metallic shield is included [33].

### 2.1.6 Fully 3-D Microwave Scanners

The 3-D microwave imaging is still a quite open area of researched in biomedical imaging. Many simulation studies have been done in the fully 3-D vectorial case [6, 34] and some experimental studies have been done with the 3-D scalar case [1, 69, 35]. Note, the difference between the scalar and vectorial case is that in a scalar case the E-field is assumed to be polarized in one dimension, while in the vectorial case the E-field polarization may vary in all three spatial dimensions. The later case makes the computations much more complex and needs a lot of calculation effort. Further, the vectorial case also introduce a complex situation in hardware development. One needs to be able to measure the E-field in two components, the horizontal and vertical polarization, to maintain the imaging algorithm with correct data. In the 2-D case or in the scalar case only one polarization of the E-filed is needed and while using a TM-wave. For the moment only Semenov *et al.* have done some initial experimental studies of the fully vectorial case [68, 36, 37, 38]. The overall goal with their 3-D studies is a full-body imaging system to detect myocardial ischemia and infarction in the human heart. In those studies two different systems have been used. The first one, was developed in the late 90s using an operating frequency of 2.36 GHz. The system is built upon a non-metallic cylindrical chamber with a diameter of 60 cm and a height of 40 cm, depicted in Figure 7. The configuration is 32 waveguide-antennas in a vertical array of transmitters with a spacing of 1 cm and the same kind of waveguide-antenna as a single receiver. The waveguide-antennas is filled with barium titanate with $\epsilon' = 60$ with the two-fold reason to minimize the antenna and matching the bolus medium

Figure 7: The first 3-D vectorial experimental setup developed by Semenov *et al.* [36], with a operating between 2.36 GHz.

to minimize the return-loss. The dimensions of the antenna is 1 x 0.5 cm with a $TE_{10}$ ($H_{10}$) wave pattern which gives a polarized field, by rotating the antenna $90^o$ the antenna is able to receive the two component polarization. [36]. While the antenna is shorter than a wavelength this waveguide-antenna may be modeled as a dipole-antenna, where the E-field in the forward direction is vertically polarized, with a reasonable accuracy in the imaging region. The scenario enable the use of a TM-wave model for relatively small objects.

This system uses a mechanical positioning system to create a circular measurement scenario by using one fixed transmitting antenna array and rotating the object and scanning with the receiving antenna $180^o$ along a circle opposite to the transmitting array. It is also possible to change the vertical position of the receiver, in between a band of 27 cm, to get multiple views along the z-axis. The positioning system has one arm for the receiving antenna and one rotator for the object. The rotator is centered in the circular chamber with the transmitting antenna array located 17.3 cm from the center. The receiving antenna is moved along a cylindrical surface with a variable radius. The E-field is then measured along a circular surface behind the object.

To speed up the data acquisition they use a code-division technique, where all transmitters may be operated simultaneously and the result is divided by the decoding system of the system [36]. However, still the data acquisition process in

this system is time consuming while the receiving antenna must measure all points on the surface at each angular position of the object, one measurement with 32 directions of a 3-D object takes about 8 h to accomplish. Another problem with the setup is that the reflection from the bottom of the chamber and the water surface must be taken into account. This occurs while calculating the result from the transmitters on the outer skirt of the antenna array, while the distance is only 4 cm between the array and the bottom and the water surface respectively.

The second generation 3-D microwave scanner developed by Semenov *et al.*, was developed in the early 2000s. This system is built around a large metallic chamber with the dimensions of 153 cm in height and 120 cm in diameter, depicted in Figure 8(a). Instead of constructing a complete transceiver the system is constructed around a network analyzer, depicted in Figure 8(c). Then only two waveguide-antennas are used together with a mechanical positioning system. the waveguide-antennas are similar to the earlier used ones with the same $TE_{10}$ mode, but is designed for frequencies between 0.8 - 1.0 GHz loaded with a core with a dielectric ($\epsilon' = 90$, $\tan\delta = 10^{-5}$). A metallic plate is fixed on the edge of both the transmitting and the receiving antenna, this to eliminate the boundary effects of the waveguide-antenna. These two antennas are fixed onto two different arms of the positioning system, depicted in Figure 8(b). During the data acquisition the object is fixed in the middle of the chamber and the positioning system rotate the antennas along a circle with the same radius for the transmitter and the receiver i.e. 18.5 cm [37]. The position system is also able to accurately locate both the

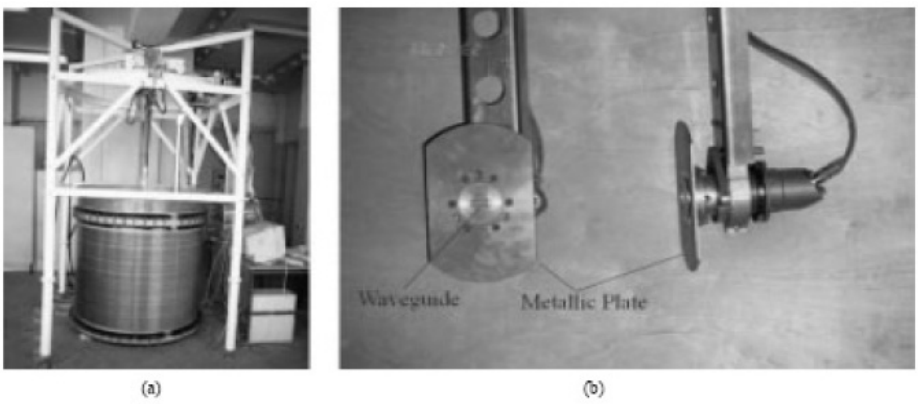


Figure 8: The second generation 3-D vectorial experimental setup developed by Semenov *et al.* [37], with a operating between 0.8 – 1.0 GHz.

transmitting and the receiving antenna in different vertical positions. By this it is possible to both receive and measure along cylindrical surfaces around objects with sizes up to 40 – 50 cm in diameter. Both antennas may automatically be rotated

during the measurements to be able to measure the two-component E-field. The system is able to measure attenuations as high as 120 dB with a signal-to-noise ratio of 40 dB. The usage of a large metallic chamber with a lossy medium makes it possible to ignore the boundary reflections and a free space boundary condition may successfully be used in the calculations.

The data acquisition may be done in three different modes. First, the simplest 2-D slice where the transmitter is located at different locations along the circle and the receiver is measuring a number of measuring points on the circle behind the object, for each transmitter position. This is the same procedure as Jofre *et al.* and Meaney *et al.* are using but in a mechanical way. Second, for each transmitting position along the circle, the receiving antenna is located along a 3-D cylindrical surface behind the object and measures the 3-D distribution of the field. In the last mode, also the transmitting antenna is located along a 3-D cylindrical surface around the object. At each transmitter location a 3-D surface measurement is done with the receiver. This measurement technique is very time consuming, while the second method with 32 transmitting positions and 18 measuring points along the circle in 16 different vertical positions of the receiver takes about 4.5 h [37]. If then also the transmitter would be located in different vertical position the number of data and the acquisition time may be multiplied with the number of vertical positions, $N_{tv}$. Using this setup this group was able to improve the image quality of fully 3-D objects, such as a full size canine [37].

## 2.2 Microwave Tomography Systems Using a Time-Domain Approach

A major part of the developed Microwave Tomography systems are designed to use one or several fixed frequencies in frequency domain. Another approach is, however, to use a multi-frequency signal in time-domain. There is mainly two groups contributing experimental results in this domain Miyakawa *et al.* and the Swedish group Persson *et al.* There solutions are completely different while Miyakawa *et al.* tries to linearize the problem to a straight line propagation problem using a chirp pulse. Persson *et al.* using a non-linear algorithm working in the time-domain.

### 2.2.1 The Chirp Pulse Microwave Computed Tomography, CP-MCT

This modality was developed by Miyakawa *et al.* This group tries only to find the straight-line projection of the traveling wave through the object, neglecting the diffraction behavior of the field. The used algorithm using the amplitude response behind the object similar to the already well-developed X-ray CT-algorithm. Filter out different traveling pathes using a static solution from an applied sinusoidal wave is impossible. Therefore, a chirp pulse with a specific sweep time is used, like a chirp radar[40, 41]. The fastest way between the transmitter and the receiver is the

straight line so the system is able to pick up the straight-line chirp pulse component from the received signal, in a spectral analysis in an FFT-analyzer [42].

The first system using this technique was developed by Miyakawa *et al.* in the early 90s. This system used two different antennas inside a saline bath and a mechanical positioning system similar to the one used in the first CT-prototype. The two antennas were moved through 128 equidistant points along two parallel lines on opposite side of the object, to measure the parallel pathes through the object. As in traditional CT this procedure was carried out at several projections along a half-circle, $180^o$. In this system they used 50 projections with $3.6^o$ intervals. Using a chirp pulse with a frequency between 1 – 2 GHz and a sweep time of 200 ms, in each measuring point the total data acquisition takes about 100 minutes. This is far too long for a clinical application, but in the initial experiment they reported approximately spatial resolution was 1 cm with the possibility to measure temperature changes as low as $0.7^o$C [40].

The data acquisition may be speed up by using simultaneous measurements with modulation scattering [40], similar to the planar microwave camera of Bolomey *et al.*. The receiver part where exchanged to one large horn-antenna with several modulated PIN diode feed dipole-antennas with multiple modulation frequencies. Using multiple modulation frequencies enables parallel measurements in several dipole positions and the system is able to accomplish faster data acquisition, the overall principle is depicted in Figure 9. However, the conclusion was that the data acquisition still was too long for a clinical application of in-vivo temperature measurements, while it needed 4.5 minutes to complete all projections.

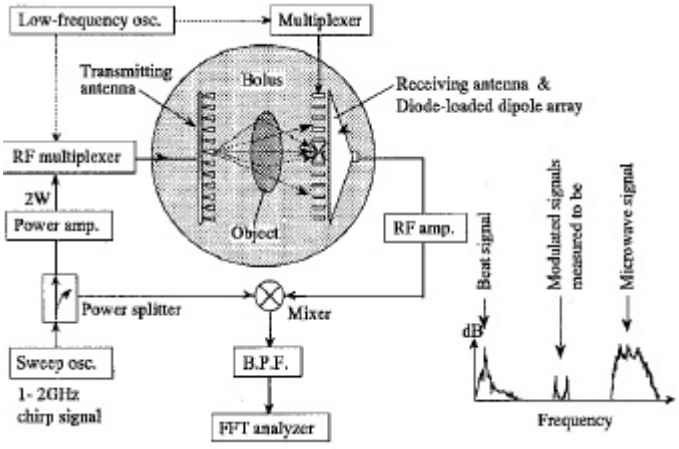


Figure 9: The hardware principle using modulated scattering and a chirp pulse, developed by Miyakawa *et al.* [40].

In the early 2000s Miyakawa *et al.* further developed their system with an

antenna array where only the circular projection scanning needs a mechanical system, depicted i Figure 10. This system consists of one transmitting dielectric loaded

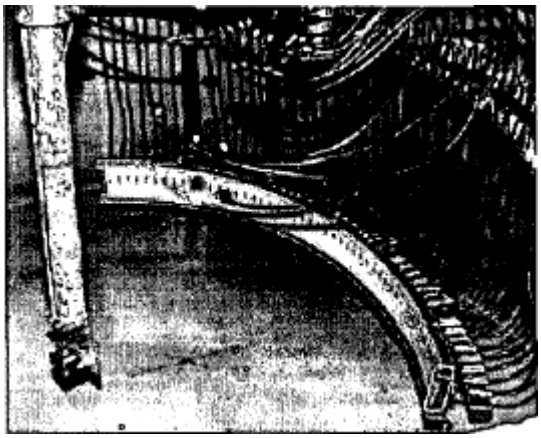

Figure 10: The fan beam scanner with 39 receiving dipole-antennas, developed by Miyakawa *et al.* [41].

waveguide-antenna with a receiving antenna array of 39 dipole antennas [41]. This system is utilized inside a saline bath using a chirp pulse from 1 – 2 GHz. Using this system a complete data acquisition of 72 projection is done in 100 seconds. If a faster system is needed, several parallel RF-signal processing units are needed. The spatial resolution of this system is between 10 – 12 mm while able to detect temperature variations of $0.3 - 0.5^{o}$C. Note, this resolution is calculated from experimental results on models and is not validated with real biological tissues.

This group has done several developments in the distinguish of the straight line path response to improve the image quality [42, 43]. The major drawback with this technique is the fact that it is really hard to distinguish the straight path only response from the received signal. The examples shown in the experimental studies are simpler structures with maximum two scatterers inside the object. Biological tissues are more complex with inhomogeneous dielectric properties, multiple scatterers with large variations in dielectric properties, which will make the imaging process even harder.

The last development progress of this technique was to adapt the system with 128 x 50 measuring points into a breast tumor detection application. In this case the frequency band where changed to 2 – 3 GHz with a variable sweep time between 20 – 200 ms [44]. In this study the detection and the positioning of an early stage breast tumor is investigated in simulations. The evaluated resolution was 6 – 7 mm, But it must be noted that it is really hard to localize the tumor from the images, even in the two-dimensional case. Therefore, the authors are suggesting that additional radar imaging is needed for the localization of the tumor, while

the chirp pulse microwave imaging technique may just be useful as a detection technique[44]. Perhaps the chirp technique is not suitable in situations where the dielectric contrast is too large, which increases the diffraction behavior of the E-field.

### 2.2.2 Time-Domain Microwave Tomography

This domain using a similar non-linear inverse scattering problem as in the single frequency setups. The difference is the wide-band multi-frequency acquisition is used to obtain time-domain data. Multi-frequency is one way to get more information about the object in the reconstruction. However one problem is that the material properties are frequency dependent, which is a challenging modeling issue in the reconstruction [46]. Persson *et. al.* has developed a wide-band circular system using monopole antennas in a frequency band between $2 - 7$ GHz [45, 46], depicted in Figure 11. This system has been developed in different stages, ex-

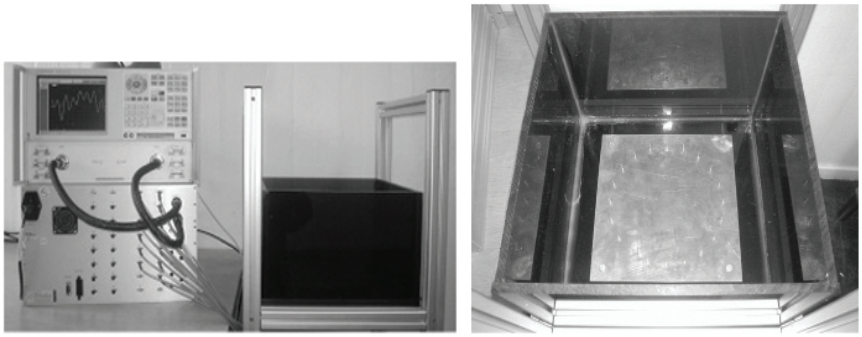


Figure 11: The circular setup for time-domain reconstruction, developed by Persson *et al.* [45].

plained in [46]. The system is built around a network analyzer and a 2:32 channel switch multiplexer. The antenna setup is similar to Meaney *et. al.* using monopole antennas. Also, a similar calibration technique is used[24, 46]. This system was used to make multi-frequency data acquisition for the time-domain inverse scattering problem. Note, FFT was used to transform the frequency domain data to time-domain.

## 2.3 Microwave Microwave Imaging Using a Radar Technique Approach

An another microwave imaging modality is developed from the already high developed microwave radar techniques. Today, a radar system may not use a rotational antenna. By using an planar array of antenna elements with variable phase-shifts (time-shift) a electronically rotation of a beam is possible. Similar techniques may be developed in the small-scale scenario of microwave imaging to detect inhomogeneities inside objects. In this area Hagness *et al.* has developed a technique to detect early breast tumors using a a Space-Time Beamforming radar.

### 2.3.1 The Space-Time Beamforming Radar approach

This technique using the reflected response, compared to the other tomographic techniques where the transmitted response are of interest. The idea is to isolate the responses from different locations with different distances from the antenna by using space-time beamforming. By computing the traveling time in time-domain using the permittivity from fatty breast tissues a time window may be used to isolate the response. Using responses from several different locations a 3-D map of the reflections may be created [47, 48]. The large reflection from the object boundary is suppressed by subtracting the average response from every location to each individual response. All antenna locations have the same distance to the object boundary, therefore this effect may be suppressed with good accuracy. However, this method may have difficulties while the response from the inhomogeneity is small compared to the reflection from the boundary of the object. This limits the solution to situations where the the purpose is to locate high contrast scatterers inside an almost homogenous object, which is the case in breast tumor detection. This group have designed an ultrawide-band (UWB) horn-antenna for this purpose [49]. The antenna has a frequency band of 1 – 11 GHz, with the aperture size of 25 x 20 mm, depicted in Figure 12. The antenna should be filled with some dielectric medium similar to breast tissues to maintain the frequency band and improve the matching against the human breast, soybean oil where suggested. This antenna has been used in an experimental investigation of breast tumor detection using this technique [50]. The breast is modeled by soybean, dielectric properties as ($\epsilon_r = 2.6$ and $\sigma = 0.05$ S/m) inside a tank with the dimensions of 36 x 36 x 26 cm. The skin layer is modeled by a 1.5 mm thick printed circuit board (PCB), while the tumor is modeled by a water-diacetin mixture inside a 4 mm diameter cylindrical plastic container with a height of 4 mm. The soybean filled horn-antenna is located at 7 x 7 matrix on the PCB, depicted in Figure 13. The results from this study indicate a great potential for this technique in detecting and positioning the breast tumor. Note that this technique only gives qualitative results of the detection and localization of a strong scatterer not the quantitative permittivity properties of the tumor, which could be useful in characterizing a tumor.

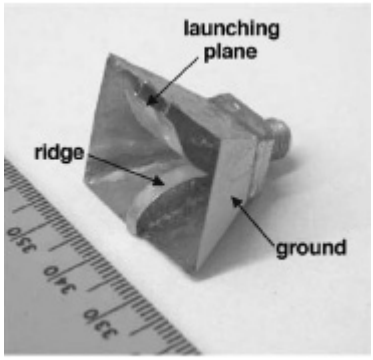


Figure 12: The 1 – 11 GHz UWB horn-antenna, developed by Hagness *et al.* [50].

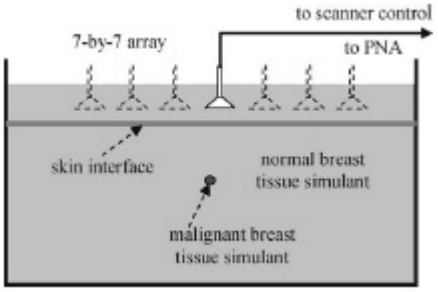


Figure 13: A cross-section of the experimental setup used by Hagness *et al.*, using soybean oil as breast tissue and coupling medium and a PCB to model the skin layer [50].

# 3 The Tomographic Algorithm Development

In the very first experimental efforts of microwave imaging a method related to X-ray formalization based on a linear path between the transmitting and receiving antenna were used [53]. However, the physical properties of microwaves makes the imaging process using microwaves more complicated compared to X-ray Computed Tomography (CT). An X-ray travels through media with a ray pattern, while the wavelength is small compared to the object size. A microwave have a wavelength similar to the object size, which makes the ray description improper describing the spread of a traveling microwave through a biomedical object. In this case the traveling wave will be highly affected by diffraction. Therefore, the diffraction effect must be involved in the imaging algorithm to obtain a quantitative result of the object.

## 3.1 The Diffraction Tomography

In the early 80s the first microwave tomography algorithms where developed, issuing the diffraction phenomenon. This was in parallel during the development of ultrasonic algorithms to obtain quantitative results of soft tissues. The main idea was to make a linear approximation of the non-linear correlation between an inhomogeneity inside the object and the received field. One approximation is to assume the electric field inside the object to be effected by the inhomogeneous object itself, called the Born approximation. In this case the solution is quite simple and the algorithms obtained with a quasi real-time performance. However, this approximation is shown valid only for smaller objects with small changes of the refractive index, e.g. weakly scattering objects [52].

In Figure 14 (left) a two-dimensional case is depicted, where a vertically polarized plane wave is illuminating a cylindrical object with an inhomogeneous cross section S with the permittivity $\epsilon_S(x, y)$ and the conductivity $\sigma_S(x, y)$. The formalization of a scenario like this may be as follows, assuming the total field $E_{tot}$ to be the sum of the incident field $E_{inc}$ and the scattered field $E_{scatt}$ according to

$$E_{tot}(x, y) = E_{inc}(x, y) + E_{scatt}(x, y). \tag{1}$$

One may also assume that the object is located in origo of the x-y plane with a plane-wave incidence along the y-axis with a wavenumber (spatial frequency) of $k_0$. The field is measured along a line parallel with the x-axis located at $y = l$, in Figure 14. If the surrounding medium is homogeneous the scattered field is generated by the equivalent currents inside the object caused by the variation of the dielectric properties. This equivalent current may be defined as

$$J_S(x, y) = (k_S^2(x, y) - k^2)E_{tot}(x, y), \qquad (x, y) \in S. \tag{2}$$

Here $k_S$ is the wavenumber inside the object and $k$ is the wavenumber of the

homogeneous surrounding medium. Note, that the wavenumbers contains the permittivity and conductivity of the object and the surrounding medium [53].

The scattered field occurred by the induced currents may be defined using the integral equation (3) or (4). By computing the convolution in this equation the forward problem solving the scattered field from the induced currents of the object is easily determined.

$$E_{scatt}(x,y) = \int\int_S J_S(x',y')G(x,y,x',y')dx'dy', \tag{3}$$

or

$$E_{scatt}(\vec{r}) = \int\int_S (k_S^2(\vec{r'}) - k^2)E_{tot}(\vec{r'})G(\vec{r},\vec{r'})dr', \tag{4}$$

where $\vec{r}$ is a general way to define the coordinates. The term $G(\vec{r},\vec{r'})$ is the two-dimensional Green's function containing the solution of the scattering problem defined by the inhomogeneous Helmholtz's equation (5).

$$(\nabla^2 + k_0)G(\vec{r},\vec{r'}) = -\delta(\vec{r} - \vec{r'}), \qquad [52]. \tag{5}$$

The delta function in the right-hand side of (5) describes a point inhomogeneity, therefore, the Green's function may be regarded to represent the effect on the field resulting from a point source. By performing the convolution, in the integral, of the Green's function over the whole region $S$ as in equation (4) the scattered field from the whole object is included. Equation (4) containing the total field inside the object, which have an unknown object interaction, which is impossible to solve without iterative methods or using some kind of approximations. This may be done using the first-order Born approximation, or the Rytov approximation not discussed in this report [52]. Consider the scattered field as a function of the total field according to equation (4) and (1), if one assumes the object as a week scatterer the incident field inside the object will be much larger than the scattered field. In that case the equivalent current inside the object may be defined as equation (6) with a constant electric field inside the object.

$$J_S(\vec{r}) = (k_S^2(\vec{r}) - k^2)E_{inc}(\vec{r}) \tag{6}$$

This results to a scattered field dependent only of the incident field, the integral formulation is then (7).

$$E_{scatt}(\vec{r}) = \int\int_S O(\vec{r'})E_{inc}(\vec{r'})G(\vec{r},\vec{r'})dr', \tag{7}$$

where $O(\vec{r}) = k_S^2(\vec{r}) - k^2$. A common and computation effective way to compute Equation (7) is to use the Fourier diffraction theorem [14, 52, 53]. The Fourier Diffraction Theorem relates the Fourier transform of the scattered field, the diffracted projection, to the Fourier transform of the object along a circular

arc. This is simply done by a Fourier transform of equation (7) into the spatial frequency domain according to equation (8).

$$\tilde{E}_{scatt}(\vec{\Lambda}) = \tilde{G}(\vec{\Lambda})\{\tilde{O}(\vec{\Lambda}) * \tilde{E}_{inc}(\vec{\Lambda})\}, \tag{8}$$

where $\vec{\Lambda} = (\alpha, \beta)$ and $(\alpha, \beta)$ are the spatial frequencies along the x- and y-axis respectively. Note, that '$*$' represent a convolution. The Fourier transform for the planar-incident wave is given by equation (9).

$$\tilde{E}_{inc}(\vec{\Lambda}) = 2\pi\delta(\vec{\Lambda} - \vec{k}_0), \tag{9}$$

where $k_0$ is the spatial frequency of the plane-wave. As well known this delta function causes a simple frequency shift in the frequency domain given by

$$\tilde{O}(\vec{\Lambda}) * \tilde{E}_{inc}(\vec{\Lambda}) = 2\pi\tilde{O}(\vec{\Lambda} - \vec{k}_0). \tag{10}$$

The Fourier transform of the Green's function is then defined as

$$\tilde{G}(\vec{\Lambda}, \vec{r'}) = \frac{e^{-j\vec{\Lambda}\cdot\vec{r'}}}{\vec{\Lambda}^2 - \vec{k}_0^2}, \qquad [52]. \tag{11}$$

Then the general Fourier transform for the scattered field may be defined as

$$\tilde{E}_{scatt}(\vec{\Lambda}) = 2\pi\frac{\tilde{O}(\vec{\Lambda} - \vec{k}_0)}{\vec{\Lambda}^2 - \vec{k}_0^2}, \tag{12}$$

where $\vec{r'} = 0$ in the Green's function. In this case it is interesting to find the scattered field along the receiver line $(x, y = l)$. As an illustration this may be calculated using the inverse Fourier transform of equation (12) according to equation (13).

$$\tilde{E}_{scatt}(x, y = l) = \frac{1}{2\pi}\int\int \frac{\tilde{O}(\alpha, \beta - k_0)}{\alpha^2 + \beta^2 - k_0^2} e^{j(\alpha x + \beta l)} d\alpha d\beta, \tag{13}$$

where y is replaced with l, which is the position of the measuring line on the y-axis. The integration is done along the line defined by equation (14), depicted in Figure 14. Since this is a forward scattering problem the negative part of $\beta$ is ignored [52]. This because the negative circular arc is related to the reflected field. Using the Fourier diffraction theorem the scattered field at the measured line in the forward scattering problem is transposed on a half circle, with positive $\beta$ values, in frequency domain with the center point at $k_0$, depicted in Figure 14.

$$\beta_{1,2} = \pm\sqrt{k_0^2 - \alpha^2} \tag{14}$$

In [52] it is described how the double integral of equation (13) may be replaced by a contour integral as equation (15) using the $\beta$ properties of (14).

$$\tilde{E}_{scatt}(x, y = l) = \int \Gamma_1(\alpha, l) e^{j\alpha x} d\alpha, \tag{15}$$

where $l$ must be larger than the object size and $\Gamma_1(\alpha; l)$ is defined as

$$\Gamma_1(\alpha; l) = \frac{\tilde{O}(\alpha, \sqrt{k_0^2 - \alpha^2} - k_0)}{j2\sqrt{k_0^2 - \alpha^2}} e^{j\sqrt{k_0^2 - \alpha^2}l}. \tag{16}$$

By taking the Fourier transform of both sides of equation (15) it results in equation (17).

$$\int \tilde{E}_{scatt}(x, y = l) e^{j\alpha x} dx = \tilde{\Gamma}_1(\alpha, l), \tag{17}$$

where the $\tilde{\Gamma}_1(\alpha, l)$ may be seen as a phase-shifted version of the object function $\tilde{O}$. Therefore, the Fourier transform of the scattered field along the measuring line at $y = l$ is related to the Fourier transform of the object function along a circular arc. This technique is called Fourier Diffraction Projection Theorem [54]. For simplicity

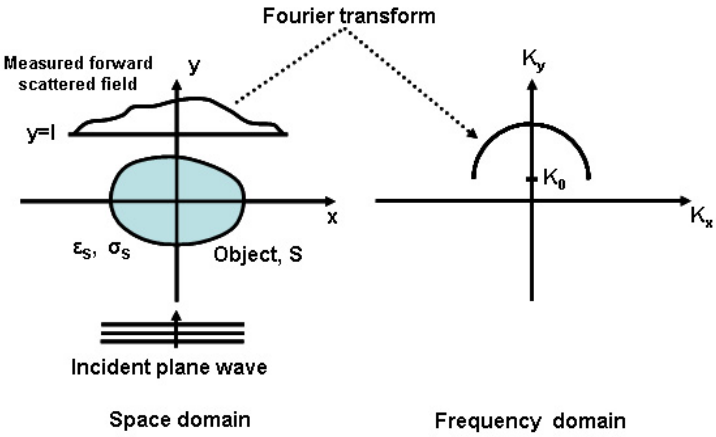


Figure 14: The Fourier diffraction theorem, [52].

only one incidence angle is issued in this document, but for further information about multiple incidence see [53]. This theorem proves the validity of the relation between weakly scattering objects and the field measured at a line. Furthermore, In [54] two different types of algorithms are presented to solve the inverse problem to estimate the object, the filtered-backpropagation algorithm and using interpolation in both frequency and spatial domain. To the author's knowledge the filtered-backproagation technique is the most commonly used, e.g. the planar microwave camera by Bolomey *et al.* [16]. This algorithm is not given in detail here but the overall principle with the filtered-backpropagation is described shortly. The filtered-backpropagation algorithm is very similar to the backpropagation algorithm for X-rays with the difference of an extra depth dependent filtering function. This filtering function is a transfer function corresponding to the depth depending attenuation

of the microwave. By using proper filter coefficients the received field may be backpropagated to illustrate the object in slices parallel to the measuring line [54].

Further, it has been shown that the limit for the validity of the Born approximation follows equation (18) [52].

$$n_\delta a < \frac{\lambda}{4}, \tag{18}$$

where $n_\delta$ is the difference in refractive index between the object and the homogenous immersing medium and $a$ is the radius of the object. The wavelength $\lambda$ is the wavelength of the planar wave in the homogenous immersing medium. However, the dielectric contrast of different human tissues are large and the objects are usually quite large. Therefore, the Born approximation is not sufficient for quantitative results, more advanced non-linear iterative algorithms are needed in this case.

## 3.2 Non-Linear Iterative Algorithms

As well known the Diffraction theorem only gives qualitative results of biological tissues, while the Born approximation fails in the most scenarios including biological in-vivo tissues. This because the multiple scattering inside the object is ignored, while the field inside the object is assumed to be homogenous and approximated to the incident field in equation (7). The difference between qualitative and quantitative results is that a qualitative result may find a difference in the dielectric properties and some position information while the quantitative result gives a more exact complex permittivity distribution of the object.

To obtain quantitative images of more complicated structures, the non-linear relation between measured scattered field and the object's dielectric properties must be taken into account. This could be done by estimating the object properties from equation (4). Note, the non-linearity arises while the effect of the scattered field is the sum of the responses from the internal object. This makes both the field inside the object and the properties of the object unknown in equation (4). This needs an iterative process to solve, which hereafter is called non-linear inverse scattering. The non-linear inverse scattering problem may be described as an optimization process where the difference between the measured field and the calculated field is minimized. When the error is sufficient small the dielectric properties in the calculations distinguish the reconstructed image of the object, depicted in Figure 15. Inverse scattering consists of three major parts. First, an appropriate physical model of the scenario. Several simplifications have been used in the developed systems, which may introduce artefact in the final result [29]. Therefore the physical modeling is a major issue during the hardware development. Second, the physical model must be implemented using a numerical method to calculate the scattered field from the known incidence field due to the assumed dielectric property of the object. This numerical process is called the forward problem, or direct problem, where the scattered field is calculated, from a known incident field, using a discrete

version of the physical model, depicted in Figure 15. Naturally this discretization may introduce some errors in the result if not a prorate decision is taken [55]. The third part is the non-linear optimization process, where iteratively the error between the measurements and the simulated fields is minimized with the goal to find the global minimum. This process is ill-conditioned and may end up in faulty local minimum if not an appropriate regularization is used [6]. All tougher those parts are working as described in Figure 15, where a known incidence field is applied to the measurements and into the forward solver. The field is measured at different points outside the object. A comparison between the calculated and measured field is then done. If the difference is larger than a specified level the inverse operation will update the permittivity distribution of the object, which then is used in the forward problem, in the next iterative step of the inverse solver. This is carried out until the error is sufficiently small and the process hopefully have found the global minimum of the non-linear problem. Note, that the initial guess $D_0$ may be used during the first iteration of the inverse process. In this chapter the three different parts will be described shortly before the overall research results and status in the area is presented.

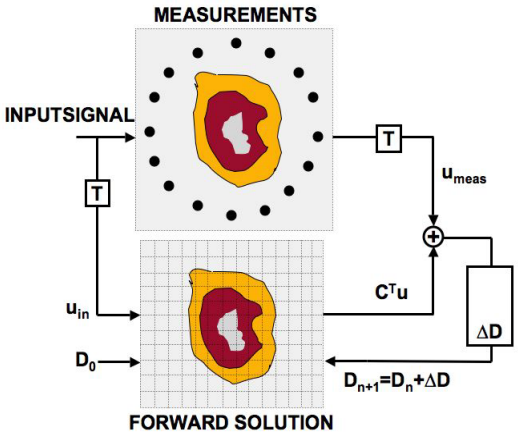


Figure 15: The concept of Microwave Imaging using inverse scattering, where the T boxes are transformations from the signal properties as amplitude and phase into the applied and received complex E-field.

### 3.2.1 The Physical Description

Using the four Maxwell equations, Equation (19)-(22) together with the three constitutive relations Equation (23)-(25) all situations concerning electro-magnetic (EM) wave propagation may be described. However, those equations are dependent

of both the E- and H- field. By taking the curl of both sides of Equation (19) or (20) and the using suitable constitutive relations it is possible to calculate the wave equation dependent on only one field component, the E- or H-field [56, 57].

$$\nabla \times H = J + \frac{\partial D}{\partial t} \tag{19}$$

$$\nabla \times E = -\frac{\partial B}{\partial t} \tag{20}$$

$$\nabla \cdot D = \rho \tag{21}$$

$$\nabla \cdot B = 0 \tag{22}$$

$$J = \sigma E \tag{23}$$

$$D = \epsilon E \tag{24}$$

$$B = \mu H \tag{25}$$

The Maxwell's equations describe the field properties in all three dimensions, which results in a calculation heavy vectorial problem in 3-D. By knowing the scenario many simplification may be done to the final wave equation, e.g. if the incidence field is vertically polarized and the object is homogenous along the z-axis. In this case the Maxwell's equations may be simplified to the scalar Helmholtz equation (26), which is used in most of the developed systems [4, 5, 6, 15, 20, 23, 58].

$$(\nabla^2 - k^2(r))E(r) = 0, \tag{26}$$

where $k$ is called the wave number containing the material properties of the medium the EM-wave is propagating trough. $E(x, y)$ is the total electric field. Other simplifications may be done by concerning the scenario as an infinite container with a homogenous immersing medium. In this case the infinite boundary conditions of the Maxwell's equation dramatically simplifies the solution of the wave equation [33].

### 3.2.2 The Forward Solution

The usual methods for the forward solver is the integral equation using Method of Moments (MoM) [4, 5, 6, 15, 58], Finite Element Method (FEM) [22, 23, 25]or in some cases Finite Difference Method (FDM) [35, 59, 45]. This document will focus on the may be most commonly used method in the literature, the integral formalization using MoM. This method were successfully used by several groups in parallel [4, 6, 58]. Those solutions are similar where the scenario where considered to accomplish the scalar Helmholtz equation (26). The solution may be expressed by the integral equation (4). The discretization of the integral equation (4) is done using MoM [56, 6, 5], which results in equation (27), defining the relation between

the total field in the object and the measured scattered field.

$$E^v_{scatt}(r_m) = \sum_{j=1}^{N}(k_S^2(r_j) - k^2)E^v_{tot}(r_j)G(r_m, r_j), \qquad m = 1, 2, \cdots, M, \tag{27}$$

where $M$ is the number of measurement points around the object and $N$ is the number of discrete cells in the solution. The term $v$ indicates the projection of the transmitting antenna [6]. The total electric field inside the object ,from the N cells, is the solution of the linear system in

$$E^v_{inc}(r_n) = \sum_{j=1}^{N}[\delta_{nj} - (k_S^2(r_j) - k^2)G(r_m, r_j)]E^v_{tot}(r_j). \qquad n = 1, 2, \cdots, N, \tag{28}$$

These two equations may be written in matrix form as equation (29) and (30).

$$[E^v_{scatt}] = [K][D][E^v_{tot}], \tag{29}$$

$$[E^v_{inc}] = [I - GD][E^v_{tot}], \tag{30}$$

where $[E^v_{scatt}]$ is a vector with length $M$ while $[E^v_{tot}]$ and $[E^v_{inc}]$ are vectors with length $N$. The $[D]$ matrix is an $N$ x $N$ diagonal matrix containing the permittivity contrast of the $N$ cells. The [K] and [G] matrix contains the Green's operator and have the sizes of $M$ x $N$ and $N$ x $N$ respectively. This technique works with the discrete version of the exact integral equation, which is normally is a accurate method if the boundary conditions are selected properly. The FEM and FDM solutions are sometimes called differential methods, which builds on approximations with local support while the integral formalization have global support [56]. The problem with integral formulations may be to define exact boundary conditions in some conditions, but in the case of microwave imaging often a infinity approximation is used in the Green function. In this case the MoM solution is simple and have the big advantage that only the object region has to be discretizised. However, the difference between the methods will not be issued in detail in this document, the interested reader may found it in literature such as [56].

### 3.2.3 The Inverse Optimization Process

The optimization process of the non-linear inverse scattering problem is a ill-posed problem without only one simple solution. The key point is to minimize the error between the measured and calculated field at the receiving antennas using a non-linear least square method, depicted in Figure 15. One may specify an object function $F$ as equation (31), which is the square norm of the difference between the measured and calculated field shown in Figure 15.

$$F(D) = \frac{||E_{scatt}(D) - E_{meas}||^2}{2} = min, \tag{31}$$

where the residual $E_{scatt}(D) - E_{meas}$ may be defined as $\Delta E_{scatt}(D)$. The term $D$ is the permittivity distribution matrix used in the forward solver as depicted in Figure 15. The goal is then to find the global minimum of this object function using the non-linear least-mean-square method. In the a general non-linear least-mean-square method,the Newton method, where both the gradient and the Hessian matrix of the object function needs to be defined [60].The gradient of the object function may be calculated as Equation (32) and the Hessian matrix as Equation (33).

$$\nabla_D F(D) = J_F^T(D)\Delta E_{scatt}(D) \tag{32}$$

$$H_F(D) = J_F^T(D)J_F(D) + \sum_{i=0}^{M} \Delta E_{scatt}^i(D) H_{\Delta E_{scatt}^i}(D), \tag{33}$$

where M is the number of observation points. The optimization is located at the minimum point when the statement in Equation (34) is approved [60].

$$H_F(D)\Delta s = -\nabla_D F(D), \tag{34}$$

where $\Delta s$ is the optimization step of the material property matrix D. The Hessian matrix defined in Equation (33) is computation heavy and it is not efficient to calculate $M$ $H_{\Delta E_{scatt}^i}(D)$ hessian matrixes in practical problems. Therefore equation (34) is often simplified by using a Gauss-Newton method as

$$J_F^T(D)J_F(D)\Delta s = -J_F^T(D)\Delta E_{scatt}(D). \tag{35}$$

This solution is very limited while the implementation does not support regularization to avoid local minima of the object function. While this non-linear problem is ill-posed the optimization needs to be controlled by regularization to suppress unwanted results in local minima with non-realistic permittivity distribution. Therefore the Levenberg-Marquardt method [1, 5, 6], (this technique is also named the Newton-Kantorovich method [5, 7]), is often used in the literature . In these techniques the Hessian approximation is extended from the Gauss-Newton , defined as Equation (36).

$$\big(J_F^T(D)J_F(D) + \mu I\big)\Delta s = -J_F^T(D)\Delta E_{scatt}(D), \tag{36}$$

where $\mu$ is often called the regularization-term used to improve the convergence of the ill-possed problem. This term is selected to improve the condition number of the Jacobian matrix $J^T J$, which stabilizes the convergence of the minimization of the object function. Large regularization-term will filter out and suppress solutions with too rapid spatial variations in the material properties. Too large regularization-term will of course limit the resolution around a high permittivity gradient inside the object. Therefore, the regularization of the optimization is a major issue during the non-linear inverse scattering in microwave imaging.

### 3.2.4 The Development of the Non-Linear Inverse Scattering in Microwave Imaging

The first non-linear inverse scattering solution where developed by different groups in parallel in the beginning of the 90s. [4, 6, 58]. All these solutions use similar integral formalization to express the scattered field in a infinite chamber. MoM is used in all cases to discretizise the investigation area of the forward problem. One slight difference between the solutions is that Chew *et al.* and Carosi *et al.* used the equivalent current formalization inside the object in the integral equation of the scattered field similar to equation (3), while Joachimowicz *et al.* and Franchois *et al.* separated the E-field and the permittivity distribution to highlight the permittivity distribution according to equation (4) and (27). All these solutions used a Levenberg-Marquardt formulation of the inverse optimization problem, while Chew *et al.* and Carosi *et al.* call the solution Distorted Born and Nadine *et al.* call their solution for Newton-Kantorovich. In [5] it is shown that both Distorted Born and Newton-Kantorovich is similar to the Levenberg-Marquardt solution. Different kinds of regularization have been proposed but it is shown that the empirically Tikkonov regularization offers the best results during high contrast objects where the initial guess differs a lot from the final unknown distribution. Further, these solutions are working with the scattered field, according to equation (37).

$$E_{scatt} = E_{tot} - E_{inc} \tag{37}$$

In practical measurements this means that first the field without the object is measured before the object is introduced int the scenario. Then the total field is measured including the object. Using equation (37) the measured scattered field from the object is calculated. Note, this is a differential measurement, which has the advantages to suppress offsets in the system and high-levels of incident field at antenna locations where the incidence field is much larger then the scattered field. Both those advantages will increase the sensitivity of the system.

In the middle of the 90s Meaney *et al.* proposed a Newton-type algorithm quite different to the earlier contributions. They were using the same Levenberg-Marquardt type of optimization with a Tikkonov regularization, but using a hybrid element forward solver instead of the earlier MoM contributions. The hybrid element (HE) solution contains of an FE mesh of the investigation area and a boundary element solution of the homogenous region outside the object. The FE method is known to be an efficient way to model inhomogeneous dielectric objects with high spatial resolution, while sparse matrixes are used in the calculations. The processor load and memory usage are reduced compared to the integral formalization with MoM in many cases. The drawback is then that the whole scenario has to be discretetisized compared to MoM where only the object region may be included. One effective way to solve this is to use the Hybrid Element (HE) method, depicted in Figure 16. The idea is to use the FE method inside the object region and use a BE integral solution of the surrounding external medium [22][23]. However, in this

method the calculations is done with the total field, which have some drawbacks in the sensitivity of object inhomogeneities at antenna positions highly influenced by the incidence field and also in suppression of offsets in the system [61]. This

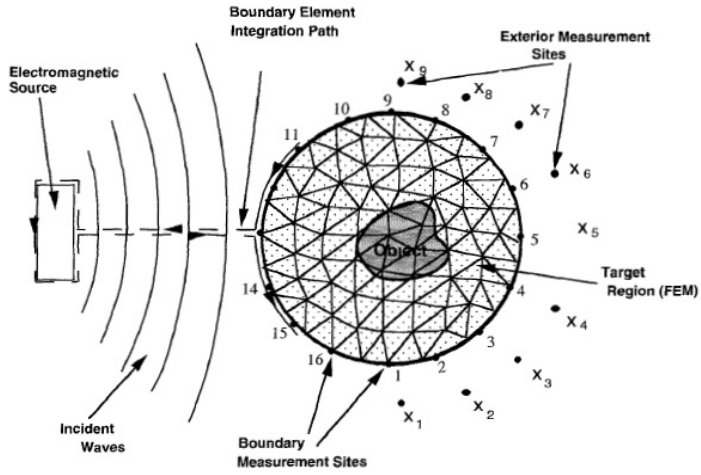


Figure 16: The conceptional illustration of hybrid element method used by Meaney *et al.* [61].

HE method has been used for breast tumor detection by microwave imaging, where the goal is to create quantitative images of the permittivity distribution inside the breast. The human breast is quite complicated to reproduce. Since, the contrast is high, between 1:2 and 1:5, between the fatty breast tissues and the object size is quite large object compared to the earlier contributions in the area. Both the size and the high contrast makes the convergence of the optimization harder while the phase will be wrapped around the unit circle. With this phenomenon the traditional algorithm losing some of the real phase information which must be solved with *a priori* information. To stabilize the convergence Meaney *et al.* developed an inverse solver which is working with the measured phase and logarithmic amplitude directly [28]. A key point in this solution is to use multiple frequencies during the measurements, starting from 300 MHz up to 1000 MHz. In a low frequency situation a wrap-around is avoided while the wavelength is in size of the complete system. By comparing the data of higher frequencies with the lower frequency data a wrap-around is detected. Another key point in this solution is to put the wrap-around into account during the calculations. Therefore, Meaney *et al.* developed a Maxwell's equations formalization where the phase is described in multiple complex Rieman sheets[28]. Interestingly, it was shown that this indeed improved the results imaging high scattering objects like breast tumors. Another improvement has been done for the breast tumor detection by finding the true boundary of the

breast before setting the hybrid element solution of the scenario. This is done by conformal microwave imaging [2]. The boundary between the FE method and the Boundary Element region is located to the boundary of the breast. In this move it is possible to set a step function at the boundary with the permittivity of the surrounding water. When the permittivity of the background medium is known the inverse problem includes only to find the permittivity of the object itself. This improved the quantitative result a lot, especially when the tumor was located near the boundary of the breast [2]. The first HE algorithm did not integrate the interaction of the antennas and the surrounding system, as the first MoM solutions but some effort has been done to take the nonactive antennas into account [62, 63]. The resulting model of the nonactive antenna is a microwave-sinc, which suppresses the wave without any reflections. Also, the MoM solvers like Newton-Kantorovitch have been improved with the interaction of the antenna coupling [64]. With this solution it is possible to use a non lossy medium and create images without the infinite approximation of the scenario.

Alternative optimizing schemes have also been investigated, the Multiplicative Regularization Contrast Source inversion by Abubakar *et. al.*[67, 69, 71], global optimization methods using neural networks, genetic algorithms and nondestructive evaluation by Caorsi *et. al.* [72, 73, 74, 75]. Those methods will not be issued in this report, but in shortly those methods avoiding local minima though the global optimization with the cost of a slower convergence and higher computation load. Until now single frequency solutions is most widely used, but different groups working on multi-frequency solutions [45, 46, 76]. It is known that the low frequencies lower the affect of non-linearities and stabilizes the algorithm, while the higher frequencies increasing the resolution, the idea is that a combination will improve the reconstruction. However, there is a frequency dependence of biological tissues and many future research efforts could focus in this area.

# 4 The Phantom Model Development

One important issue of microwave imaging of biological tissues is the phantom models. It is important to use a phantom which is able to indicate the ability to reconstruct the dielectric properties of the human tissues. This document will concentrate on the breast tumor detection application. While it is mainly the Meany *et al.* and the Hagness *et al.* who contributes this area the presented models here is contributions from their research. Table 1 shows recommended properties by the literature used by Hagness *et al.*. This numbers indicate a ration of 5:1 between the tumor and the surrounding breast tissues. However Meaney *et al.* propose in [25] that this number may be as low as 2:1 in real *in vivo* measurements while the water content is much higher in the breast tissues in this case. This propose is grounded by the mean permittivity values reconstructed from measurements on real patients. In Figure 17 a model used by Hagness *et al.* is depicted, using *ex-vivo* material

| Tissue | $\epsilon_r$ | $\sigma$ | Frequency |
|---|---|---|---|
| Skin | 36 | 4 | @ 2.5 GHz |
| Breast Tissue | 9 | 0.4 | @ 2.5 GHz |
| Tumor | 50.0 | 4 | @ 2.5 GHz |

Table 1: Dielectric properties of human tissues [65].

properties refereed in the literature. This model was used in FDTD simulations to

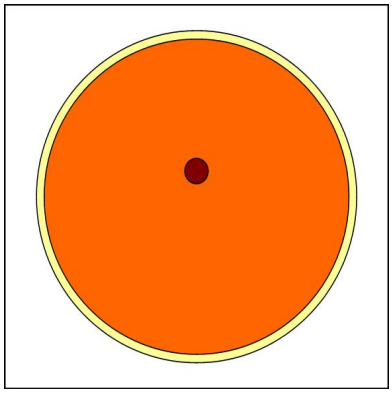

Figure 17: A 2D model used by Hagness *et al.* [65]. The breast model diameter is 68 mm wich a skin layer of 2 mm and a tumor diameter of 6 mm. The material properties used is presented in Table 1. The background medium is selected to $\epsilon_r = 9$ and $\sigma = 0$.

verify the Space-Time Beamforming radar algorithm. Meaney *et al.* has used a 2D

model for both simulations and real experiments. Figure 18 depicts a simple 2D model used by Meaney *et al.*. In this model the skin layer is ignored and the ration between the breast tissues and the tumor is only 2:1. The material properties used is $\epsilon_r = 77$ and $\sigma = 1.6$ @ 900 Mhz for the background medium and tumor inclusion. The Breast tissues is modeled by a water (21%), corn syrup (78%) and agar (1%) mixture $\epsilon_r = 35$ and $\sigma = 0.7$. The size of the model is 82 mm in diameter with a 19 mm diameter tumor located 23 mm off-center in the phantom However, Meaney

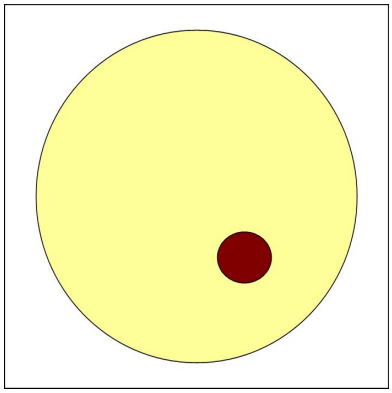

Figure 18: A simple 2D model used by Meaney *et al.* [2].

*et al.* has also created a more advanced 3D model used in simulations, depicted in Figure 19. This model containing the inhomogeneities of fiber granules inside the breast with a 6 mm diameter spherical tumor inside.

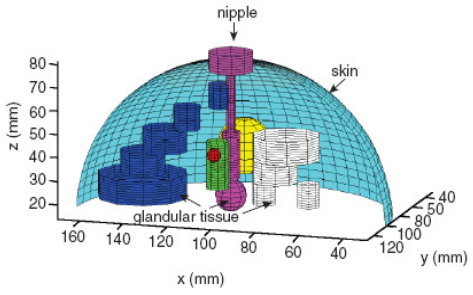


Figure 19: The 3D model with fiber granules with a diameter of 140 mm and a 6 mm diameter spherical tumor, used by Meaney *et al.* [65].

Those examples are the mainly contributions in the phantom area of breast tumor detection. The exact *in-vivo* complex permittivity seems to be not settled yet while the properties variate between different patients with different blood flow, different age and rate of fatty tissue inside the breast. However a expected contrast between 1.5-5:1 seems to be settled [50].

# 5 Discussion and Future Work

Imaging of biological tissues is one of the most challenging application area of microwave imaging. This is mostly because of the high permittivity contrast of biological tissues and the complex geometrical structure. In many industrial application the diffraction tomography using the Born approximation is well suited with its computational effectiveness. However, in the most cases of biological imaging the non-linear multiple scattering inside the object must be taken into account. Because, the size and contrast are to big to appropriately use the Born approximation. Several groups have put a lot of effort to solve the ill-posed non-linear inverse problem. The other approach, using radar techniques the detection and localization of strong scatters are possible. However, while the author believe that the quantitative complex permittivity reconstruction may be useful in the decision e.g. if the tumor is malign, the iterative non-linear inverse scattering solution is preferred.

At the moment mostly 2D slices in the TM-case have been investigated. Some approaches have been done to use a scalar 3D algorithm in a TM-wave system, by Meaney *et al.* Also Semenov *et al.* have tried to produce 3D solutions using a vectorial 3D algorithm with promising results. In the authors opinion, it could be interesting to use the Newton-Kantorovich based on MoM in the breast tumor case, to se the usability of these algorithms in this area. By transform the algorithm to the 2.45 GHz planar microwave camera located at Supélec as Ann Franchois, further quantitative investigations may be done of inhomogeneous objects. While the retina of the planar camera measures the vertical electric field, it may be useful in the 3D case by rotating the retina 90 degrees measuring both vertical and horizontal polarized E-field. The earlier 2D system developed by Meaney textitet al. suffers from several 3D/2D artifacts. By using the planar camera in 3D configuration further 3D investigation may be done.

# 6 Conclusions

In this document the historical development of the biomedical imaging using microwaves is issued. Several hardware systems have been developed with different aims some more successful than others. However, the main issue of this document is the application of breast tumor detection using microwave imaging. In this area it is mainly two groups with active research, Meaney *et al.* and Hagness *et al.*.

They have complectly different approach around the problem where Meaney *et al.* using nonlinear microwave tomography to create quantitative permittivity images, while Hagness *et al.* tries to find the tumor using radar techniques. The radar approach may be useful while it may be easier to realize as a clinical system for detection and positioning of the tumor more easily, but it may not be able to create permittivity information about the scatterer it self, i.e. if the tumor is malign or not. Therefore, the author indicates the interest to further develop the microwave tomography for this purpose. The system today uses 2-D models for the imaging purpose. The more calculation loaded 3-D case is therefore of interest. By applying the non-linear inverse scattering to a modified planar microwave camera, located at Supélec, fully 3-D investigation may be performed.

# References


[1] Q. Fang, P. M. Meaney, S. D. Geimer and A. V. Streltsov, "Microwave Image Reconstruction From 3-D Fields Coupled to 2-D Parameter Estimation," *IEEE Transactions on Medical Imaging*, Vol-23, No. 4, pp. 475–484, April 2004.

[2] D. Li, P. MMeaney and K. D. Paulsen, "Conformal Microwave Imaging for Breast Cancer Detection," *IEEE Transactions on Mircorwave Theory and Techniques*, Vol-51, No. 4, pp. 1179–1186, April 2003.

[3] P. M. Meaney, Q. Fang, E. Demidenko and K. D. Paulsen, "Error Analysis in Microwave Breast Imaging: Variance Stabilizing Transformations," *Procedingc of ICONIC 2005*, UPC Barcelona, Spain, pp. 67–71, June 2005.

[4] W. C. Chew and Y. M. Wang,"Reconstruction of Two-Dimensional Permittivity Distribution Using the Distorted Born Iterative Method," *IEEE Transactions on Medical Imaging*, Vol-9, No. 2, pp. 218–225, April 2004.

[5] A. Franchois, C. Pichot"Microwave Imaging–Complex Permittivity Reconstruction with a Levenberg-Marquardt Method," *IEEE Transactions on Antennas and Propagation*, Vol-45, No. 2, pp. 203–215, February 1997.

[6] N. Joachimowicz, C. Pichot and J. -P. Hugonin, "Inverse Scattering: An Iterative Numerical Method for Electromagnetic Imaging," *IEEE Transactions on Antennas and Propagation*, Vol-395, No. 12, pp. 1742–1752, December 1991.

[7] N. Joachimowicz, J. J. Mallorqui, J. -C. Bolomey and A. Broquetas, "Convergence and Stability Assessment of Newton–Kantorovich Reconstruction Algorithms for Microwave Tomography," *IEEE Transactions on Medical Imaging*, Vol-17, No. 4, pp. 562–570, August 1998.

[8] A. E. Bulyshev, A. E. Souvorov, S. Y. Semenov, V. G. Posukh and Y. E. Sizov, "Three-dimensional vector microwave tomography theory and computational experiments," *Institute of Physics Publishing, Inverse Problems*, No. 20, PII: S0266-5611(04)72896-8, pp. 1239–1259, 2004.

[9] A. Abubakar, P. M. van den Berg and S. Y. Semenov, "Two- and Three-Dimensional Algorithms for Microwave Imaging and Inverse Scattering," *Journal of Electromagnetism Waves and Applications*, Vol-17, No. 2, pp. 209–231, 2003.

[10] L. E. Larsen and J. H. Jacobi, "Mcrowave Scattering Parameter Imaging od an Isolated Canine Kidney," *Medical Physics*, Vol-6, pp. 394–403, 1979.

[11] Bolomey J. C. Gardiol Fred E. "Engineering Applications of the Modulated Scatterer Technique", [Series: Artech House Antennar and Propagation Library], ISBN: 1580531474.

[12] A. Joisel, J. Mallorqui, A. Broquetas, J. M. Geffrin, N. Joachimowicz, M. V. Iossera, L. Jofre and J. -C. Bolomey, "Microwave Imaging Techniques for Biomedical Applications," *Instrumentation and Measurement Technology Conference*, 1999.

[13] J. -C. Bolomey, L. Jofre and G. Peronnet "On the Possible Use of Microwave-Active Imaging for Remote Thermal Sensing," *IEEE Transactions on Mircorwave Theory and Techniques*, Vol-31, No. 9, pp. 777–781, September 1983.

[14] C. Rius, C. Pichot, L. Jofre, J. -C. Bolomey, N. Joachimowicz, A. Broquetas and M. Ferrando, "Planar and Cylindrical Active Microwave Temperature Imaging: Numerical Simulations," *IEEE Transactions on Medical Imaging*, Vol-11, No. 4, pp. 457–469, December 1992.

[15] A. Franchois, A. Joisel, C. Pichot and J. -C. Bolomey, "Quantitative Microwave Imaging with a 2.45-GHz Planar Microwave Camera," *IEEE Transactions on Medical Imaging*, Vol-17, No. 4, pp. 550–561, August 1998.

[16] A. Joisel and J. -C. Bolomey, "Rapid Microwave Imaging of Living Tissues," *SPIE Symposium on Medical Imaging San Diego*, CA, USA, February 12-18, 2000.

[17] L. Jofre, M. S. Hawley, A. Broquetas, E. De Los Reyes, M. Ferrando and A. R. Elias-Fuste, "Medical Imaging with a Microwave Tomographic Scanner," *IEEE Transactions on Biomedical Engineering*, Vol-37, No. 3, pp. 303–311, March 1990.

[18] A. Broquetas, J. Romeu, J. M. Rius, A. R. Elias-Fuste, A. Cardama and L. Jofre, "Cylindrical Geometry: A Further Step in Active Microwave Tomography," *IEEE Transactions on Mircorwave Theory and Techniques*, Vol-39, No. 5, pp. 836–844, May 1991.

[19] A. Abubakar, P. M. van den Berg and J. J. Mallorqui, "Imaging of Biomedical Data Using a Multiplicative Regularized Contrast Source Inversion Method," *IEEE Transactions on Mircorwave Theory and Techniques*, Vol-50, No. 7, pp. 1761–1771, July 2002.

[20] S. Y. Semenov, R. H. Svenson, A. E. Boulyshev, A. E. Souvorov, V. Y. Borisov, Y. Sizov, A. N. Starostin, K. R. Dezern, G. P. Tatsis and V. Y. Baranov, "Microwave Tomography: Two-Dimensional System for Biomedical Imaging," *IEEE Transactions on Biomedical Engineering*, Vol-43, No. 9, pp. 869–877, September 1996.

[21] P. M. Meaney, K. D. Paulsen, A. Hartov and R. K. Crane, "An Actice Microwave Imaging System for Reconstruction of 2-D Electrical Property Distributions," *IEEE Transactions on Biomedical Engineering*, Vol-42, No. 10, pp. 1017–1025, October 1995.

[22] P. M. Meaney, K. D. Paulsen and T. P. Ryan, "Two-Dimensional Hybrid Element Image reconstruction for TM Illumination," *IEEE Transactions on Antennas and Propagation*, Vol-43, pp. 239–247, 1995.

[23] K. D. Paulsen, P. M. Meaney, M. J. Moskowitz and J. M. Sullivan, "A Dual Mesh Scheme for Finite Element Based Reconstruction Algorithms," *IEEE Transactions on Medical Imaging*, Vol-14, No. 3, pp. 504–514, Mars 1995.

[24] P. M. Meaney, K. D. Paulsen and J. T. Chang, "Near-Field Microwave Imaging of Biologically-Based Materials Using a Monopole Trenceiver System," *IEEE Transactions on Mircorwave Theory and Techniques*, Vol-46, No. 1, pp. 31–43, January 1998.

[25] P. M. Meaney, M. W. Fanning, D. Li, S. P. Poplack and K. D. Paulsen, "A Clinical Prototype for Active Microwave Imaging of the Breast," *IEEE Transactions on Mircorwave Theory and Techniques*, Vol-48, No. 11, pp. 1841–1853, November 2000.

[26] K. D. Paulsen, P. M. Meaney, "Nonactive Antenna Compensation for Fixed-Array Microwave Imaging–Part I: Model Development", *IEEE Transactions on Medical Imaging*, Vol. 18, pp. 496–507, June 1999.

[27] P. M. Meaney, K. D. Paulsen, J. T. Chang, M. W. Fanning, and A. Hartov, "Nonactive Antenna Compensation for Fixed-Array Microwave Imaging Part II:–Imaging Results", *IEEE Transactions on Medical Imaging*, Vol. 18, pp. 508–518, June 1999.

[28] P. M. Meaney, K. D. Paulsen, B. W. Pogue and M. I. Miga, "Microwave Image Reconstruction Utilizing Log-Magnitude and Unwrapped Phase to Improve High-Contrast Object Recovery," *IEEE Transactions on Medical Imaging*, Vol-20, No. 2, pp. 104–116, February 2001.

[29] P. M. Meaney, K. D. Paulsen, S. D. Geimer, S. A. Haider and M. W. Fanning, "Quantification of 3-D Field Effects During 2-D Microwave Imaging," *IEEE Transactions on Biomedical Engineering*, Vol-49, No. 7, pp. 708–720, July 2002.

[30] D. Li, P. M. Meaney, T. Raynolds, S. A. Pendergrass, M. W. Fanning and K. D. Paulsen, "A BROADBAND MICROWAVE BREAST IMAGING SYSTEM," *2003 IEEE 29th Annual Biomedical Conference, Proceeding of*, pp. 83–84, Mars 2003.

[31] J. M. Geffrin J. J. Mallorqui, N. Joachimowicz R. Redondo, M. Vall-Ilossera, O. Franza, A. Joisel and J. -C. Bolomey, "REDUCTION OF THE MODEL NOISE IN NON-LINEAR RECONSTRUCTION VIA AN EFFICIENT CALCULATION OF THE INCIDENT FELD : APPLICATION TO A 434 MHz

SCANNER," *Antennas and Propagation Society 1999 IEEE International Symposium*, Vol-2, pp. 996–999, July 1999.

[32] J. M. Geffrin and A. Joisel, "Comparison of Measured and Simulated Incident and Scattered Fields in a 434 Mhz Scanner," *Procedingc of the 22th URSI General Asambly 2002*, Maastricht, The Netherlands, 17-24 August 2002.

[33] A. Franchois and A. G. Tijhuis, "A Newton-Type Reconstruction Algorithm for a 434 Mhz Microwave Imaging Scanner," *Procedingc of the 22th URSI General Asambly 2002*, Maastricht, The Netherlands, 17-24 August 2002.

[34] S. Caorsi, A. Massa and M. Pastorino, "A Numerical Solution to Full-Vector Electromagnetic Scattering by Three-Dimensional Nonlinear Bounded Dielectrics," *IEEE Transactions on Mircorwave Theory and Techniques*, Vol-43, No. 2, pp. 1841–1853, February 1995.

[35] P. M. Meaney, Q. Fang, S. D. Geimer, A. V. Streltsov and K. D. Paulsen, "3D Scalar Microwave Image Reconstruction Algorithm," *Microwave Symposium Digest, 2002 IEEE MTT-S International*, Vol-3, pp. 2269–2272, 2-7 June 2002.

[36] S. Y. Semenov, R. H. Svenson, A. E. Boulyshev, A. E. Souvorov, A. G. Nazarov, Y. E. Sizov, A. Pavlovsky, V. Y. Borisov, B. A. Voinov, G. I. Simonova, A. N. Starostin, V. G. Posukh, M. Taran, G. P. Tatsis, and V. Y. Baranov, "Three-Dimensional Microwave Tomography: Experimental Prototype of the System and Vector Born Reconstruction Method," *IEEE Transactions on Biomedical Engineering*, Vol-46, No. 8, pp. 937–946, August 1999.

[37] S. Y. Semenov, R. H. Svenson, A. E. Boulyshev, A. E. Souvorov, V. Y. Borisov, A. G. Nazarov, Y. E. Sizov, V. G. Posukh, A. Pavlovsky, P. N. Repin, A. N. Starostin, B. A. Voinov, M. Taran, G. P. Tatsis, and V. Y. Baranov, "Three-Dimensional Microwave Tomography: Initial Experimental Imaging of Animals," *IEEE Transactions on Biomedical Engineering*, Vol-49, No. 1, pp. 55–63, January 2002.

[38] S. Y. Semenov, A. E. Boulyshev, A. E. Souvorov, A. G. Nazarov, Y. E. Sizov, R. H. Svenson, V. G. Posukh, A. Pavlovsky, P. N. Repin and G. P. Tatsis, "Three-Dimensional Microwave Tomography: Experimental Imaging of Phantoms and Biologocal Objects," *IEEE Transactions on Microwave Theory and Thechniques*, Vol-48, No. 6, pp. 1071–1074, June 2000.

[39] S. Y. Semenov, R. H. Svenson, A. E. Boulyshev, A. E. Souvorov, A. G. Nazarov, Y. E. Sizov, V. G. Posukh, A. Pavlovsky, P. N. Repin and G. P. Tatsis, "Spatial Resolution of Microwave Tomography for Detection of Myocardial Ischemia and InfarctionExperimental Study on Two-Dimensional Models," *IEEE Transactions on Microwave Theory and Thechniques*, Vol-48, No. 4, pp. 538–544, April 2000.

[40] M. Miyakawa and T. Hayashi, "An Atemt of High-Speed Imaging of the Chirp Radar-Type Microwave Computed Tomography," *Microwave Symposium Digest, 1997., IEEE MTT-S International,* Vol-1, pp. 115–118, June 8-13, 1997.

[41] M. Miyakawa, E. Harada and W. Jing,"Chirip Pulse Microwave Computed Tomography(CP-MCT) Equipped with a Fan Beam Scanner for High-speed Imaging of a Biological Target," *Proceedings of the 25 Annual lntemational Conference of the IEEE EMBS,* Caneun, Mexico, September 17-21, 2003.

[42] M. Bertero, M. Miyakawa, P. Boccacci, F. Conte, K. Orikasa and M. Furutani, "Three-Dimensional Microwave Tomography: Initial Experimental Imaging of Animals," *IEEE Transactions on Biomedical Engineering*, Vol-47, No. 5, pp. 690–699, May 2000.

[43] M. Miyakawa, K. Orikasa, M. Bertero, P. Boccacci, F. Conte and M. Piana, "Experimental Validation of a Linear Model for Data Reduction in Chirp-Pulse Microwave CT," *IEEE Transactions on Medical Imaging*, Vol-21, No. 4, pp. 385–395, April 2002.

[44] M. Miyakawa, T. Ishida and M. Watanabe,"Imaging Capability of an Early Stage Breast Tumor by CP-MCT," *Procedingc of the 26th Annual International Conference of the IEEE EMBS San Francisco,* CA, USA, September 1-5, 2004.

[45] A. Fhager, P. Hashemzadeh, and M. Persson, "Reconstruction Quality and Spectral Content of an Electromagnetic Time-Domain Inversion Algorithm", *IEEE Transactions on Biomedical Engineering*, Vol-53, No. 8, pp. 1594–1604, August 2006.

[46] A. Fhager, " Microwave Tomography," Ph.D. Thesis, *Department of Signals and Systems, Chalmers Univerity of Technology*, 2006.

[47] E. C. Fear, X. Li and S. C. Hagness, "Confocal Microwave Imaging for Breast Cancer Detection: Localization of Tumors in Three Dimensions," *IEEE Transactions on Biomedical Engineering*, Vol-49, No. 8, pp. 812–822, August 2002.

[48] J. Bond, X. Li and S. C. Hagness "Microwave Imaging via Space-Time Beamforming for Early Detection of Breast Cancer," *IEEE Transactions on Antennas and Propagation*, Vol-51, No. 8, pp. 1690–1705, August 2003.

[49] J. Bond, X. Li and S. C. Hagness "Numerical and Experimental Investigation of an Ultrawideband Ridged Pyramidal Horn AntennaWith Curved Launching Plane for Pulse Radiation," *IEEE Antennas and Wireless Propagation Letters*, Vol-2, pp. 259–262, 2003.

[50] X. Li, S. K. Davis, S. C. Hagness, D. W. van der Weide and B. D. Van Veen, "Microwave Imaging via SpaceTime Beamforming: Experimental Investigation

of Tumor Detection in Multilayer Breast Phantoms," *IEEE Transactions on Mircorwave Theory and Techniques*, Vol-52, No. 8, pp. 1856–1865, August 2004.

[51] J. -C. Bolomey, A. Izadnegahdar, L. Jofre, C. Pichot, G. Peronnet and M. Solaimani, "Microwave Diffraction Tomography for Biomedical Applications," *IEEE Transactions on Mircorwave Theory and Techniques*, Vol-30, No. 11, pp. 1998–1982, November 1982.

[52] M. Slaney, A. C. Kak, and L. E. Larsen, "Limitations of Imaging with First-Order Diffraction Tomography," *IEEE Transactions on Mircorwave Theory and Techniques*, Vol-32, No. 8, pp. 860–874, August 1984.

[53] C. Pichot, L. Jofre, G. Peronnet and J. -C. Bolomey, "Active Microwave Imaging of Inhomogeneous Bodies," *IEEE Transactions on Antennas and Propagation*, Vol-33, No. 4, pp. 416–423, April 1985.

[54] S. X. Pan and A. C. Kak, "A Computational Study of Reconstruction Algorithms for Diffraction Tomography: Interpolation Versus Filtered Backpropagation," *IEEE Transactions on Acoustics, Speech and Signal Processing*, Vol-31, No. 5, pp. 1262–1275, October 1983.

[55] N. Joachimowicz and C. Pichot, "Comparison of Three Integral Formulations for the 2-D TE scattering Problem," *IEEE Transactions on Mircorwave Theory and Techniques*, Vol-38, No. 2, pp. 178–184, February 1990.

[56] M. V. K. Chari, S. J. Salon, "Numerical Methods in Electromagnetism, " Academic Press, ISBN: 0-12-615760-X, 2000.

[57] R. F. Harrington, "Time-Harmonic Electromagnetic Fields, " IEEE Press, ISBN: 0-471-20806-X.

[58] S. Caorosi, G. L. Gragnani and M. Pastorino, "Two-Dimensional Microwave Imaging by a Numerical Inverse Scattering Solution," *IEEE Transactions on Mircorwave Theory and Techniques*, Vol-38, No. 8, pp. 981–989, August 1990.

[59] W. C. Chew G. P. Otto, W. H. Weedon, J. H. Lin, Y. M. Wang and M. Moghaddam, "Nonlinear Diffraction Tomography—The Use of Inverse Scattering for Imaging," *Conference Record of The Twenty-Seventh Asilomar Conference on Signals, Systems and Computers, 1993.*, Vol-1, pp. 120–129, 1-3 November 1993.

[60] M. T. Heath, "Scientific Computing, " Second Edition, Mc Graw Hill, ISBN: 0-07-112229-X, 2002.

[61] P. M. Meaney, K. D. Paulsen, A. Hartov and R. K. Crane, "Microwave Imagng fr Tissue Assessment: Initial Evaluation in Multitarget Tissue-Equivalent Phantoms," *IEEE Transactions on Biomedical Engineering*, Vol-43, No. 9, pp. 878–890, September 1996.

[62] K. D. Paulsen and P. M. Meaney, "Nonactive Antenna Compensation for Fixed-Array Microwave Imaging—Part I: Model Development," *IEEE Transactions on Medical Imaging*, Vol-18, No. 6, pp. 496–506, June 1999.

[63] P. M. Meaney, K. D. Paulsen, J. T. Chang, M. W. Fanning and A. Hartov, "Nonactive Antenna Compensation for Fixed-Array Microwave Imaging: Part II—Imagng Results," *IEEE Transactions on Medical Imaging*, Vol-18, No. 6, pp. 508–518, June 1999.

[64] O. Franza, N. Joachimowicz and J. -C. Bolomey, "SICS: A Sencor Interaction Compensation Scheme for Microwave Imaging," *IEEE Transactions on Antennas and Propagation*, Vol-50, No. 2, pp. 211–216, February 2002.

[65] E. C. Fear, P. M. Meaney and M. A. Stuchly, "Microwaves for Breast Cancer Detection," *IEEE Potentials*, pp. 12–18, February 2003.

[66] A. E. Souvorov, A. E. Bulyshev, S. Y. Semenov, R. H. Svenson, A. G. Nazarov, Y. E. Sizov, and G. P. Tatsis, "Microwave Tomography: A Two-Dimensional Newton Iterative Scheme," *IEEE Trans. Microwave Theory and Tech.*, vol. 46, pp. 1654–1659 , Nov. 1998.

[67] S. Y. Semenov, A. E. Bulyshev, A. Abubakar, V. G. Posukh, Y. E. Sizov, A. E. Souvorov, P. M. van den Berg, and T. C. Williams, "Microwave-Tomographic Imaging of the High Dielectric-Contrast Objects Using Different Image-Reconstruction Approaches," *IEEE Trans. Microwave Theory and Tech.*, vol. 53, pp. 2284–2294 , July 2005.

[68] A. E. Bulyshev, A. E. Souvorov, S. Y. Semenov, V. G. Posukh and Y. E. Sizov, "Three-dimensional vector microwave tomography: theory and computational experiments," *Inverse Problems*, vol. 20, pp. 1239-1259, 2004.

[69] A. Abubakar P. M. van den Berg and S. Y. Semenov "TWO- AND THREE-DIMENSIONAL ALGORITHMS FOR MICROWAVE IMAGING AND INVERSE SCATTERING," *J. of Electromagn. Waves and Appl.*, Vol. 17, pp. 209–231, 2003.

[70] S. Caorsi, A. Massa, and M. Pastorino "A Numerical Solution to Full-Vector Electromagnetic Scattering by Three-Dimensional Nonlinear Bounded Dielectrics," *IEEE Trans. Microwave Theory and Tech.* , vol. 43, pp. 428–436 , Feb. 2005.

[71] A. Abubakar, P. M. van den Berg, and J. J. Mallorqui "Imaging of Biomedical Data Using a Multiplicative Regularized Contrast Source Inversion Method," *IEEE Trans. Microwave Theory and Tech.*, vol. 50, pp. 1761–177 , Jul. 2005.

[72] S. Caorsi and P. Gamba, "Electromagnetic Detection of Dielectric Cylinders by a Neural Network Approach," *IEEE Trans. Geoscience Remote Sens.*, vol. 37, pp. 820–827, Mar. 1999.

[73] M. Pastorino, A. Massa, and S. Caorsi, "A Microwave Inverse Scattering Technique for Image Reconstruction Based on a Genetic Algorithm," *IEEE Trans. Instrumen. Measure.*, vol. 49, pp. 573–578, June 2000.

[74] M. Pastorino, S. Caorsi, A. Massa, and A. Randazzo, "Reconstruction Algorithms for Electromagnetic Imaging," *IEEE Trans. Instrumen. Measure.*, vol. 53, pp. 692–699, June 2004.

[75] M. Pastorino, S. Caorsi, and A. Massa, "A Global Optimization Technique for Microwave Nondestructive Evaluation," *IEEE Trans. Instrumen. Measure.*, vol. 51, pp. 666–673, Aug. 2002.

[76] Q. Fang, P. M. Meaney, and K. D. Paulsen, "Microwave Image Reconstruction of Tissue Property Dispersion Characteristics Utilizing Multiple-Frequency Information," *IEEE Trans. Microwave Theory and Tech.*, vol. 52, pp. 1866–1875, Aug. 2004.